Magnetotransport properties of $La_{0.7}Sr_{0.3}MnO_3/SrTiO_3$ superlattices

L. M. Wang, Jing-Kae Lin, and Jong-Pyng Shyu
Department of Electrical Engineering, Da-Yeh University, Chang-Hwa 515, Taiwan
(Received 18 May 2006; revised manuscript received 21 August 2006; published 7 November 2006)

The crystalline structures, magnetisms, and magnetotransport properties of $La_{0.7}Sr_{0.3}MnO_3/SrTiO_3$ (LSMO/STO) superlattices and $La_{0.7}Sr_{0.3}MnO_3$ (LSMO) films are studied. The transmission electron microscopy images confirm the sharp interfaces and uniformly continuous layers in superlattices and provide the evidence that the superlattices almost have the same in-plane stress while they have a slight increase of out-of-plane strain in LSMO layers for superlattices with thicker STO layers. For the LSMO/STO superlattices with thicker STO or thinner LSMO layers, the decreases in Curie temperature, magnetization, and effective carrier concentration, accompanied by an enhanced residual resistivity, have been observed. In the magnetotransport study, the temperature dependence of longitudinal resistivity $\rho_{xx}(T)$, the magnetoresistance ratio (MR) as a function of magnetization M, and the scaling of anomalous Hall coefficient R_s versus longitudinal resistivity ρ_{xx} are found to follow the behaviors of $\rho_{xx}(T) \sim T^{\alpha}$ with $\alpha = 2.3-2.5$, $\mathrm{MR} = -C[M/M_s]^2$ with $C = 1.45-2.17$, and $-R_s \propto (\rho_{xx})^n$ with $n = 1.55-2.04$, respectively, where M_s is the saturation magnetization. Furthermore, the increased α, and the decreased C and n for superlattices with thicker STO or thinner LSMO layers, are presented. This study provides insight into the effects of decoupling and magnetic disordering on the physical mechanism of the magnetotransport properties of the LSMO/STO superlattices. Our results demonstrate that the interlayer decoupling increases the influence of disorder effects on the magnetism and dominates the magnetotransport phenomenon in LSMO/STO superlattices, while the strain effect plays a minor role on the magnetotransport properties of the overall samples discussed here.

DOI: 10.1103/PhysRevB.74.184412 PACS number(s): 75.47.Lx, 75.70.Cn, 73.21.Cd

I. INTRODUCTION

The magnetotransport properties of the compounds $R_{1-x}D_xMnO_3$ (R=rare earth, D=Ca, Sr, Ba, and Pb) have been a subject of great interest. In particular, the observations of a colossal negative magnetoresistance (CMR) accompanying a metal-insulator transition near the Curie temperature T_C have drawn immense interest for a variety of applications such as spin-electronic devices[1] and thermometers.[2] Fundamental physics of the CMR property are usually explained by introducing the double exchange mechanism, in which hopping of e_g electrons occurs between Mn^{3+} and Mn^{4+} ions through intervening filled oxygen $2p$ states.[3] In addition, there are other mechanisms that have provided valuable insight into the CMR phenomenon in the manganites, such as the antiferromagnetic superexchange, Jahn-Teller effects, as well as orbital and charge ordering.[4] The knowledge of the crystal structure and the chemical bonding of these compounds is of capital importance to the understanding of the peculiar magnetotransport properties in these perovskites. For manganite films, which have great potential for applications in the design of electronic devices, the situation becomes more complicated by containing the strain due to lattice mismatch between the substrate and the film. It has been found that properties such as magnetoresistance, magnitude of T_C, and magnetization are sensitive to the epitaxial strain in manganite films and can be controlled by depositing films on various substrates, changing the deposition parameters, or varying the thickness.[5–7] In addition to the strain effects, however, it has been suggested that the transition temperatures are also influenced by other factors, such as inhomogeneities and disorder.[8] Recently Dvorak *et al.*[9] presented evidence that T_C and saturation magnetization (M_s) are suppressed for all $La_{2/3}Ca_{1/3}MnO_3$ films as the thickness decreases, regardless of the strain within the film. This implies that strain effect is not sufficient to describe the magnetotransport in manganite films.

The manganite-based multilayers or superlattices, consisting of alternate stacking of ferromagnetic conductive layers with nonmagnetic insulating layers, have stimulated considerable interest and active studies. Previous studies have revealed a variety of physical properties such as interfacial strain effect,[10] magnetic interlayer coupling,[11] and exchange bias effect.[12] Lu *et al.*[10] have shown that the electrical transport properties and the magnetoresistance of $La_{2/3}Ba_{1/3}MnO_3/SrTiO_3$ superlattices are strongly affected by the biaxial strain. However, Izumi *et al.*[11] demonstrated the effects of spin canting in $La_{0.6}Sr_{0.4}MnO_3$ and possible electron hopping across $SrTiO_3$ layers on the electronic properties of $La_{0.6}Sr_{0.4}MnO_3/SrTiO_3$ superlattices by ruling out the strain effect. Obviously, some characteristics of transport in manganite-based films still require further investigation.

In this work, the effects on magnetotransport in $La_{0.7}Sr_{0.3}MnO_3/SrTiO_3$ (LSMO/STO) superlattices grown onto $LaAlO_3$ substrates are studied. High-quality crystalline structures have been characterized by transmission electron microscopy (TEM) and x-ray diffraction. The magnetizations, resistivities, and Hall effects are measured and analyzed to qualify the magnetotransport properties. For comparison, single layer epitaxial $La_{0.7}Sr_{0.3}MnO_3$ (LSMO) films grown on $LaAlO_3$ (LAO) and $SrTiO_3$ (STO) substrates have also been fabricated and characterized.

II. EXPERIMENTS

LSMO/STO superlattices with a 600-Å-thick STO buffer layer grown on (001) LAO substrates were prepared in a rf

magnetron sputtering system as previously described.[13] LSMO and STO layers were alternatively deposited at 700 °C in 300-mTorr sputtering gas (Ar and O_2, 3:7) until the desired thickness of a superlattice was reached. After deposition, oxygen gas at 1 atmospheric pressure was introduced into the chamber. The cooling rate was 5 °C/min and the superlattices were maintained at the growth temperature for 1 h before the cooling process. Sharp interfaces and uniformly continuous layers in superlattices were confirmed by TEM (Philips TECNAI F20). The compositions of LSMO layers were analyzed by an energy-dispersive spectrometer and showed almost stoichiometric values for samples.[13] The epitaxial growth of superlattices was characterized by an x-ray diffractometer (Shimazu XRD6000) using Cu-K_α radiations. For transport measurements, films were photolithographically patterned to a 100-μm long, 50-μm wide bridge containing six Hall and resistivity terminals. Six gold pads were evaporated onto the contact areas to ensure good electrical contact for the simultaneous transverse Hall and longitudinal resistivity measurements using the standard four-terminal method. Here, the contact pads were attached to the sample edges in order to achieve an injection of the measuring current parallel to the layers of the heterostructure. The geometry for resistivity and Hall coefficient measurements was similar to that previously shown for the transport measurements of artificial $YBa_2Cu_3O_y/PrBa_2Cu_3O_y$ superlattices,[14] in which a larger dimension of bridge was used. The magnetizations of films were measured by a superconducting quantum interference device magnetometer. In addition, two 800-Å-thick single-layer LSMO films respectively grown on LAO and STO substrates were also fabricated and characterized using the same experimental processes.

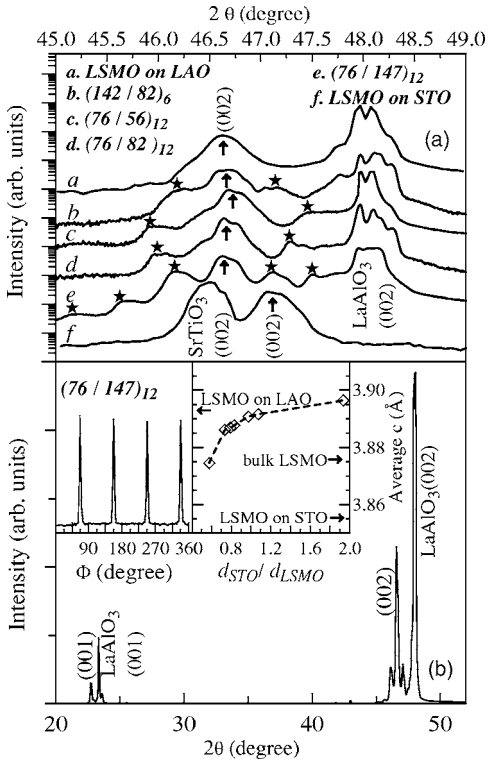

FIG. 1. X-ray θ-2θ diffraction spectra (a) in the region near the (002) peak for a series of LSMO/STO superlattices and LSMO films, and (b) in a wide-range scan for sample $(76/147)_{12}$. The satellite peaks in (a) are indicated by star symbols. The left and middle insets of (b) show the x-ray Φ-scanning on the pseudocubic (103) LSMO diffraction peak for $(76/147)_{12}$ superlattice and the average c-axis lattice constant versus the d_{STO}/d_{LSMO} ratio, respectively.

III. RESULTS AND DISCUSSION

A. Crystal structure and magnetic properties

Figure 1(a) shows the x-ray θ-2θ diffraction spectra in the region near the (002) peak for a series of LSMO/STO superlattices and LSMO films. The presence of the satellite peaks on both sides of the main peak (002) for LSMO/STO superlattices confirms that a periodic structure in the superlattices has been achieved. The superlattices are denoted by $(d_{LSMO}/d_{STO})_m$, where the numbers of d_{LSMO} and d_{STO} in parentheses correspond, respectively, to the thicknesses of LSMO and STO layers in unit of angstrom, and the subscript m denotes the total repeated number of bilayers. Figure 1(b) shows the x-ray θ-2θ scan for sample $(76/147)_{12}$, in which only the (001) and (002) diffraction peaks of film were observed, also indicating that the film has c-axis epitaxial growth. Furthermore, the in-plane orientation of the superlattices has been studied by x-ray Φ-scanning on the pseudocubic (103) LSMO diffraction peak. As can be seen, the left inset of Fig. 1(b) shows a fourfold-symmetry pattern for the $(76/147)_{12}$ superlattice. The fourfold symmetry of this pattern clearly indicates the in-plane epitaxial structure and large-scale crystalline homogeneity of the $(76/147)_{12}$ superlattice. In Fig. 1(a), the 2θ position of the (002) peak, which corresponds to the out-of-plane lattice constant, is dependent on the layer thickness in LSMO/STO superlattices and the substrate used for LSMO films. The pseudocubic lattice constants of LAO, STO and LSMO are 3.790, 3.905, and 3.876 Å,[15] respectively. Thus the LAO and STO substrates provide an in-plane biaxial compressive stress of −2.22% and an in-plane biaxial tensile stress of +0.75%, respectively. This results in a larger c-axis lattice constant (3.893 Å) and a smaller c-axis lattice constant (3.856 Å) than the bulk value of 3.876 Å for LSMO films deposited on LAO and STO substrates, respectively, as shown in the middle inset of Fig. 1(b). The middle inset of Fig. 1(b) also shows the average c-axis lattice constant versus the d_{STO}/d_{LSMO} ratio. As shown, for a superlattice with thicker STO layers or thinner LSMO layers, an enhanced average c-axis lattice constant can be observed. This feature is similar to that observed in LSMO/STO superlattices grown on STO substrates.[16] However, it is noted that the average c-axis lattice constant obtained from the x-ray diffraction cannot completely reflect the strain of the LSMO layers in superlattices. By considering the superposition of the x-ray diffraction contributed from the individual STO and LSMO layers, the d_{STO}/d_{LSMO}-ratio dependence of average c-axis lattice constant might be calculated by $c=(c_{STO}\cdot d_{STO}+c_{LSMO}\cdot d_{LSMO})/(d_{STO}+d_{LSMO})$,[16] where c_{STO} and c_{LSMO} are

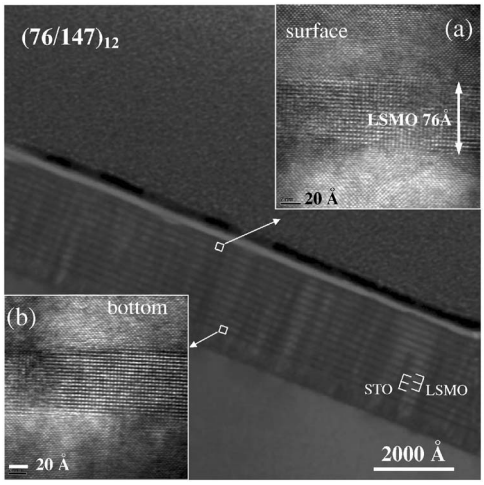

FIG. 2. Low-magnification cross-section image of $(76/147)_{12}$ superlattice. Insets (a) and (b) show the high-resolution cross-section TEM images extracted from the regions near the top surface and bottom of the bilayer stacking, respectively.

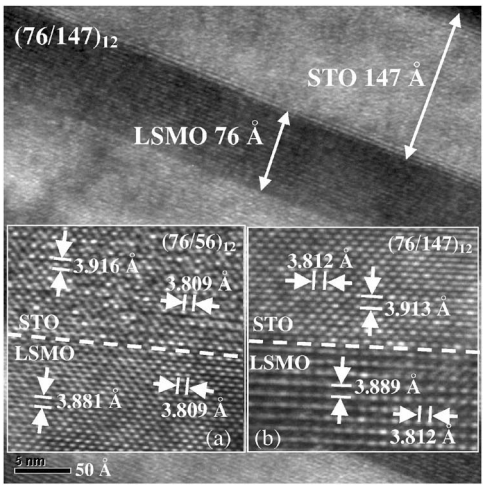

FIG. 3. High-resolution cross-sectional TEM image of the $(76/147)_{12}$ superlattice. Insets (a) and (b) show the interfaces TEM lattice images for the $(76/56)_{12}$ and $(76/147)_{12}$ superlattices, respectively.

the individual out-of-plane lattice constants in STO and LSMO layers, respectively. Thus the average c increasing with increasing d_{STO}/d_{LSMO} ratio is naturally expected since $c_{STO} > c_{LSMO}$. Further detailed structure analysis was carried out with high-resolution TEM to obtain the c_{LSMO} and thus the information of strain of LSMO layers. Figure 2 shows a typical low-magnification cross-section image of $(76/147)_{12}$ superlattice. As can be seen, the heterostructure exhibits perfect epitaxy with sharp and well-defined interfaces between successive LSMO and STO layers within a large area, which is similar to that observed by other workers.[11,17] The insets of Figs. 2(a) and 2(b) show the high-resolution cross-section TEM images extracted from the regions near the top surface and bottom of the bilayer stacking, respectively. As seen, no significant variation of microcrystalline structure can be observed, indicating that the strain state should be conserved in the whole of bilayer stacking. The strain state probed by the TEM images will be analyzed and discussed later. Recently, it was pointed out that the strain state depends on the method of growing, e.g., rf sputtering or pulsed laser deposition.[18,19] In particular, rf-sputtered $La_{0.7}Ca_{0.3}MnO_3$/STO films may be obtained in the coherently strained state for thickness up to 180 nm.[20] The observation of a coherent strain state without strain relaxation in our rf-sputtered superlattices seems to be unsurprising and consistent with those obtained by others. Figure 3 shows a high-resolution cross-sectional TEM image located at the middle part of the stacked $(76/147)_{12}$ superlattice. This figure also shows a perfectly heterostructural growth with sharp interfaces between LSMO and STO as previously reported on the $(76/56)_{12}$ superlattice.[13] Furthermore, the TEM analysis shows that the superlattice maintains the in-plane crystal coherency at the interfaces as shown in the insets of Figs 3(a) and 3(b) for $(76/56)_{12}$ and $(76/147)_{12}$ superlattices, respectively. The in-plane lattice constants of 3.809 and 3.812 Å respectively for $(76/56)_{12}$ and $(76/147)_{12}$ superlattices range just between the lattice constant of 3.79 Å of the LAO substrate and the pseudocubic lattice constant of 3.876 Å of bulk LSMO, indicating that both the LSMO and STO (a axis=c axis=3.905 Å) layers have an in-plane compressive stress state due to a smaller lattice constant of substrate. Furthermore, it can be seen that the in-plane lattice constants of 3.809 and 3.812 Å are near 3.79 Å of the LAO substrate, implying that the in-plane strain is mainly induced by the LAO substrate in the whole of stacked layers. Normally along the film there can be seen a slightly incoherent growth with individual out-of-plane lattice constants of 3.881 and 3.916 Å respectively for LSMO and STO layers in the $(76/56)_{12}$ superlattice as shown in the inset of Fig. 3(a). This corresponds to a slight elongation of the c axis by 0.005 Å in the LSMO layers and an elongation of the c axis by 0.011 Å in the STO layers. For the $(76/147)_{12}$ superlattice, the inset of Fig. 3(b) shows a similar result with individual out-of-plane lattice constants of 3.889 and 3.913 Å for LSMO and STO layers, respectively. This corresponds to a elongation of the c axis by 0.013 Å in the LSMO layers and an elongation of the c axis by 0.008 Å in the STO layers. Based on these TEM results and focusing attention on the variation of lattice constant in the LSMO layers, we can see that the superlattices have almost the same in-plane stress, while having a slight increase of out-of-plane strain in LSMO layers for superlattices with thicker STO layers. On the other hand, it can be seen that the c axis of LSMO layers obtained from the TEM image is smaller than that estimated from the x-ray diffraction. This indicates a somewhat reduced out-of plane strain of the LSMO layers in comparison to the results of x-ray diffraction and agrees with the inference proposed by Sahana *et al.*,[16] in which the values of average c axis were calculated by assuming strongly strained LSMO layers, and the values deviated from the measured values by x-ray diffraction. Here, a direct observation of TEM images provides the evidence of coherent in-plane strain in LSMO/STO superlattices and confirms a somewhat increased out-of-plane strain within the LSMO layers for superlattices with thicker STO layers.

Figures 4(a) and 4(b) show the temperature dependence of the field-cooled magnetization measured in 500 Oe for two

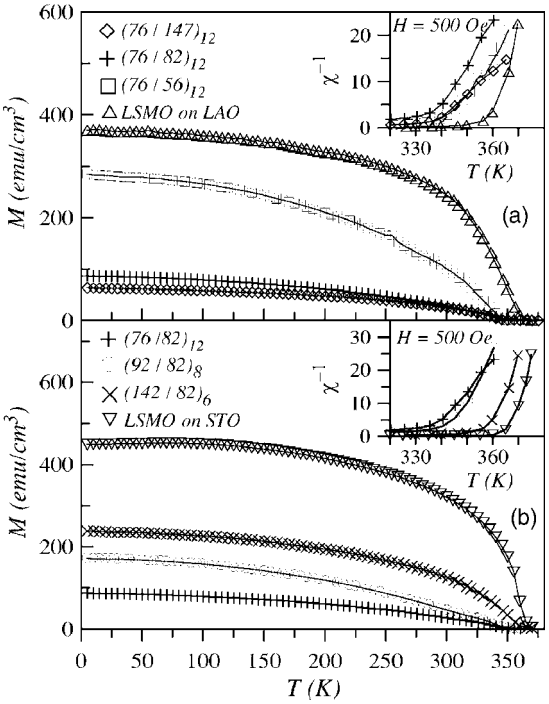

FIG. 4. Temperature dependence of the field-cooled magnetization for two series of LSMO/STO superlattices and the single-layer LSMO films. The insets show the temperature dependence of magnetic susceptibility $1/\chi$ for the corresponding samples shown in (a) and (b), respectively.

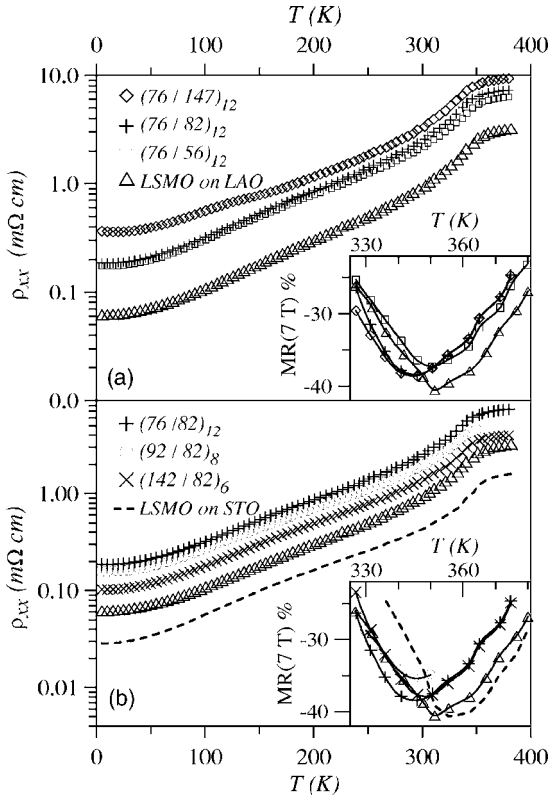

FIG. 5. Zero-field longitudinal resistivities ρ_{xx} as a function of temperature for two sets of LSMO/STO superlattices and LSMO films. The insets illustrate the temperature dependence of the magnetoresistance ratio MR (7 T) for the corresponding samples shown in (a) and (b).

series of LSMO/STO superlattices and the single-layer LSMO films. As can be seen, all the samples undergo a paramagnetic-to-ferromagnetic phase transition and the low-temperature magnetization decreases for superlattices with thicker STO or thinner LSMO layers. The insets of Figs. 4(a) and 4(b) show the temperature dependence of reciprocal magnetic susceptibility $1/\chi$ for the corresponding samples shown in Figs. 4(a) and 4(b), respectively. It is found that the Curie temperature T_C, deduced from the paramagnetic Curie temperature θ, which is determined by extrapolating linearly the temperature dependence of reciprocal magnetic susceptibility $1/\chi$ at temperatures near T_C $(T/T_C<5\%)$ in the paramagnetic state and is expected to be near T_C, decreases with increasing d_{STO} or with decreasing d_{LSMO}. The variance of Curie temperature T_C has been tabulated elsewhere.[21] The observed decrease of T_C is in agreement with those values reported in Refs. 11 and 16. It is noteworthy that for a single LSMO layer the values of low-temperature magnetization and T_C are around 400 emu/cm^3 and 360 K, respectively, regardless of the substrates used. That is, the LSMO films deposited on LAO and STO reveal a similar magnetic property even though they have different strain styles. Note that the strain relaxation should not be induced in our rf-sputtered LSMO films with a thickness of 800 Å, as mentioned before. Thus, it appears that the strain effect cannot completely interpret the decreases of magnetization and T_C observed in the LSMO/STO superlattices. Recently the magnetic properties of the manganite-based multilayers[22,23] or the III-V-based semiconducting heterostructure system[24] have been widely studied. The observed decrease of magnetic moment for multilayers with thicker space layers have been found to be strongly related to the interlayer coupling mediated by the space layers. In particular, it has been shown that the insulating space layers will enhance the decoupling and magnetic disordering among the multilayers, thereby leading to a large quenching of the magnetic moment.[22,23] Thus the decoupling and magnetic disordering seem to play a crucial role in the physical mechanism of the magnetotransport properties for the LSMO/STO superlattices. In the following, we discuss the transport properties of LSMO/STO superlattices, which are expected to be influenced by their magnetic behavior.

B. Longitudinal magnetotransport properties

Figures 5(a) and 5(b) show the zero-field longitudinal resistivities ρ_{xx} as a function of temperature for two sets of LSMO/STO superlattices and LSMO films. The insets of Figs. 5(a) and 5(b) illustrate the temperature dependence of the magnetoresistance ratio (MR), defined as MR(7 T) $=[\rho_{xx}(H=7\ \mathrm{T})-\rho_{xx}(H=0)]/\rho_{xx}(H=0)$, for the corresponding samples. It can be seen that with decreasing d_{LSMO} or increasing d_{STO}, the value of ρ_{xx} increases, and ρ_{xx} reveals a metallic state at low temperatures for all superlattices. Also visible in the insets of Figs. 5(a) and 5(b) is that a maximum −MR(7 T) value occurs near the Curie temperature for all the superlattices and the single-layer LSMO films. The maxi-

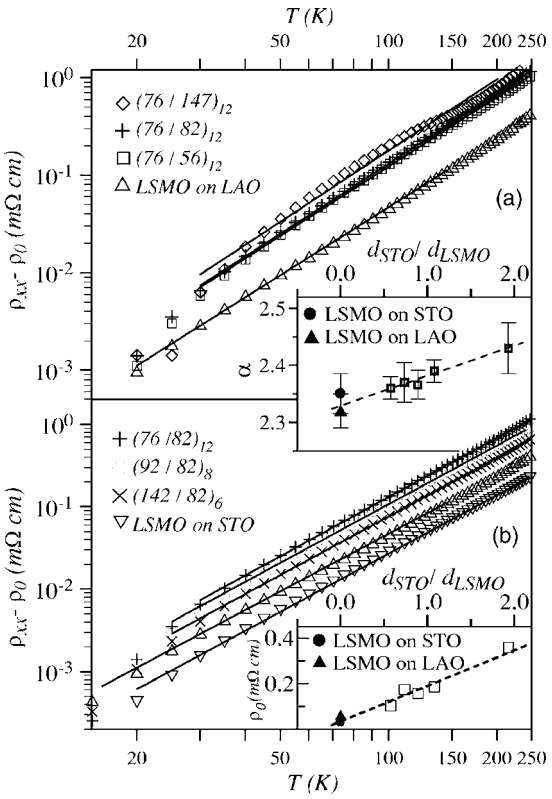

FIG. 6. The power-law temperature dependence of the resistivity fitted by $\rho_{xx}=\rho_0+AT^{\alpha}$ for two sets of LSMO/STO superlattices and LSMO films. Insets (a) and (b) show the exponent α and the residual resistivity ρ_0 versus the $d_{\mathrm{STO}}/d_{\mathrm{LSMO}}$ ratio, respectively. The dashed lines are to serve as visual guides.

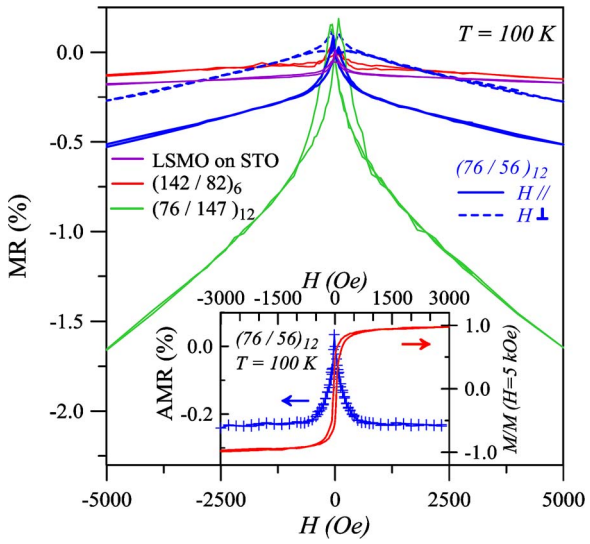

FIG. 7. (Color online) MR ratio vs external magnetic field H for some superlattices and a LSMO film measured at 100 K. Inset: the hysteretic AMR curve associated with the normalized magnetization M/M (H=5 kOe) of the $(76/56)_{12}$ superlattices performed at 100 K.

mum −MR(7 T) values for LSMO/STO superlattices occurring at temperatures of 340–350 K are in the range of 35–38%, which is slightly smaller than that of 40.5% at 351 K for the LSMO film deposited on LAO substrate. It can also be noted that both the LSMO films deposited on LAO and STO substrate exhibit residual resistivities close to that reported on the single-crystal sample,[25] and show a maximum −MR(7 T) of around 40.5%, regardless of the different types of strain within them. Added to this, it is known that the low-temperature resistivities of manganites in the ferromagnetic state are essential in investigating the mechanism of transport properties. At low temperatures, a dominant T^2 term in the resistivity has generally been observed in the manganites and can be ascribed to electron-electron scattering,[25] one-magnon scattering processes in the minority band,[26] small-polaron transport,[27] or current-carriers-density collapse.[28] Moreover, a careful check of the low-temperature resistivity has shown a substantial deviation from the T^2-dependent behavior,[5,29–33] which can be attributed to the contribution of anomalous single-magnon scattering[30] ($\rho_{xx}\sim T^3$), two-magnon scattering[29,30] ($\rho_{xx}\sim T^{9/2}$), or spin-wave scattering[31] ($\rho_{xx}\sim T^{7/2}$). Figures 6(a) and 6(b) illustrate the power-law temperature dependence of the resistivity for two sets of LSMO/STO superlattices and LSMO films. As can be seen, the resistivity can be fitted by $\rho_{xx}=\rho_0+AT^{\alpha}$ within the temperature range of 30–200 K, where the residual resistivity ρ_0 is taken with the resistivity measured at the lowest temperature of 5 K, and A and α are free parameters. It is found that the exponent α, being in the range $2.3<\alpha<2.5$, slightly increases with an increase of $d_{\mathrm{STO}}/d_{\mathrm{LSMO}}$ ratio as shown in the inset of Fig. 6(a). The evaluated values of α are close to those reported by other researchers.[32,33] The inset of Fig. 6(b) shows the residual resistivity ρ_0 versus the $d_{\mathrm{STO}}/d_{\mathrm{LSMO}}$ ratio. As can be seen, the values of residual resistivity ρ_0 are always less than 0.4 mΩ cm and also increase when the $d_{\mathrm{STO}}/d_{\mathrm{LSMO}}$ ratio increases. It is known that the residual resistivity can reflect the quality of the samples and can be considered a measure of the global disorder. Our observation of the exponent α slightly increasing with the increase of residual resistivity on LSMO/STO superlattices is in accordance with that recently reported on the manganite thin films.[33] There it was shown that the increase of α with ρ_0 is independent of the film thicknesses, the strain distribution, and the growth technique. The same is true of this case as comparing the results of single-layer LSMO films grown onto STO and LAO substrates. Both the LSMO films show a lower ρ_0 of ~0.05 mΩ cm and a lower α value of ~2.34 regardless of the strain type within them, while the disorder is enhanced in the superlattices. Apparently, the effect of disorder should be significantly considered to understand the transport properties of these LSMO/STO superlattices. As previously inferred from the magnetic properties, the magnetic disorder should be enhanced in the superlattice as the STO layers become thicker or the LSMO layers become thinner. The higher magnetic disorder associated with the magnon scattering will naturally cause the enhancement of residual resistivity observed on the superlattices.

Figure 7 shows the curves of MR versus external magnetic field H for selected samples measured at 100 K. The MR is calculated by $\mathrm{MR}(H)=[\rho_{xx}(H)-\rho_{xx}(0)]/\rho_{xx}(0)$ with the magnetic field parallel ($H\|$) or perpendicular ($H\perp$) to the electric current. Here, the measurements were done with

magnetic fields applied in the film plane to eliminate the demagnetization effect. As can be seen, the $(76/147)_{12}$ superlattice shows a more rapid decrease of MR, that is, a more strongly magnetic-field dependence of resistance than that observed in other sample. The obvious field dependence of resistivity can be regarded as a feature of the contribution from the electron-magnon scattering of minority-band carriers as observed on the $La_{0.67}(Pb,Ca)_{0.33}MnO_3$ single crystals[26] and $SrRuO_3$ films.[34] Of course, this magnon-scattering process will become significant if the minority spin states appear and the spin polarization decreases. Indeed, a strongly reduced spin polarization deduced from the anisotropic magnetoresistance (AMR) results for the $(76/147)_{12}$ superlattice has be presented elsewhere.[13] This also confirms the claim that for the larger values of disorder,[33] such as observed on the $(76/147)_{12}$ superlattice, the temperature scaling of resistivity tends toward the law T^3 characteristic of anomalous single magnon scattering process as previously shown in the inset of Fig. 6(a). Another noteworthy feature shown in Fig. 7 is that the butterfly-shaped MR curves in the low-field region are clearly observed for $(76/56)_{12}$ and $(76/147)_{12}$ superlattices, implying that tunneling through the STO space layers also plays a minor role within the electrical transport. The lower inset of Fig. 7 shows the hysteretic AMR curve associated with the normalized magnetization $M/M(H=5\ \text{kOe})$ of the $(76/56)_{12}$ superlattices performed at 100 K, where the AMR is estimated by $\text{AMR}=\text{MR}(H\|)-\text{MR}(H\perp)$. It can be seen that the AMR remains nearly constant as the magnetization becomes saturated, while an anomalous AMR behavior appears at low fields. Considering that the magnetization is not fully aligned in the low-field region, the low-field AMR is considered to contain an extrinsic contribution originating from the grain-boundary or interfacial disorder at various interfaces.[23,35] The nearly field-independent AMR observed in the high-field region also indicates that the Lorentz force effect is suppressed by the insulating STO layers in the $(76/56)_{12}$ superlattice. It is known the Lorentz force bends the trajectory of the carriers and then contributes a positive MR at high fields for the transverse configuration. If the Lorentz mechanism dominates the AMR at high fields, it may be expected that the AMR value will be negative and will decrease with increasing fields according to the definition of AMR $=\text{MR}(H\|)-\text{MR}(H\perp)$. This result indicates that the magnetoresistance contributed from the Lorentz force effect can be suppressed by the insulating STO space layers and thus the AMR behavior is controllable by the artificial superlattices.

To further clarify the mechanism of magnetotransport properties, it is essential to understand the correlation between the resistivity and magnetization. Figure 8 displays the relationship between the MR and magnetization in the low-M regime. As can be seen, the MR can be described by $\text{MR}(H)=-C[M(H)/M_s]^2$, where C is a dimensionless coefficient, and the saturation magnetization M_s is measured with $H=20$ kOe at 5 K. The magnetization dependence of MR was obtained using the $\rho_{xx}(T)$ and $M(T)$ data which were both measured with $H=5$ kOe parallel to the current and the film plane, respectively. The origin of $\text{MR}\propto M^2$ can be explained by carrier scattering due to the thermally fluctuating

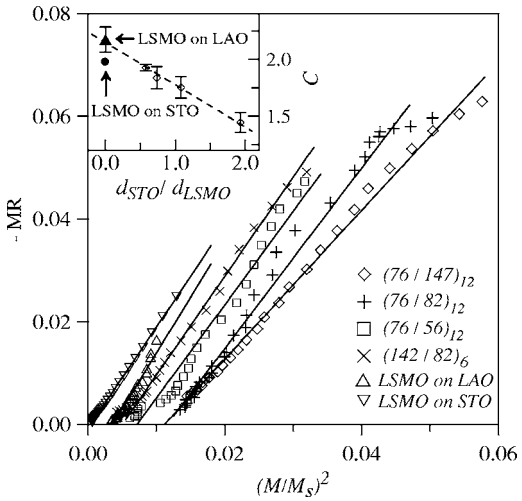

FIG. 8. The MR vs magnetization in the low-M regime for the LSMO/STO superlattices and LSMO films. The solid lines indicate the relationship of $\text{MR}(H)=-C[M(H)/M_s]^2$. The magnetization dependence of MR was obtained using the $\rho_{xx}(T)$ and $M(T)$ data, which were both measured with $H=5$ kOe parallel to the current and the film plane, respectively. The inset shows the coefficient C versus the $d_{\text{STO}}/d_{\text{LSMO}}$ ratio, and the dashed line is to serve as a visual guide.

spins, or spin-disorder scattering. When induced magnetic moment is developed, the amplitude of the spin fluctuation decreases so that the resistivity $\rho_{xx}(H)$ decreases, and therefore the magnitude of MR increases. Furukawa[36] has calculated the coefficient C in terms of the Kondo lattice model with ferromagnetic exchange interaction and showed that it is related to the coupling between moving carriers and the localized spins, i.e., the Hund coupling. The calculated value of C is about 4–5 in the case of strong coupling, but the value becomes $C\approx 1$ at the weak coupling limit. As seen in the inset of Fig. 8, the coefficient C is in the range of 1.45–2.17 and decreases with an increase of $d_{\text{STO}}/d_{\text{LSMO}}$ ratio, indicating that the coupling becomes weaker for superlattices with thicker STO layers or thinner LSMO layers. This result is consistent with the inference from the low-temperature properties of AMR and magnetization discussed elsewhere,[13] in which a reduced exchange coupling, leading to an incomplete polarization of the carriers, has been observed on LSMO/STO superlattices with thicker STO layers or thinner LSMO layers. It can be noted that both the values of coefficient C for single-layer LSMO films deposited on STO and LAO substrates are near the value of 2.0, again indicating that the strain effect has only a minor affect on the magnetotransport properties of the overall samples discussed here.

C. Transverse Hall resistivities

Figures 9(a) and 9(b) show the typical results of the transverse Hall resistivity ρ_{xy} versus applied field H for the LSMO film deposited on LAO and the $(76/82)_6$ LSMO/STO superlattice at different temperatures, respectively. The $\rho_{xy}(H)$ curves exhibit similar characteristics as those observed in other doped manganese-oxide perovskites,[37–39] and

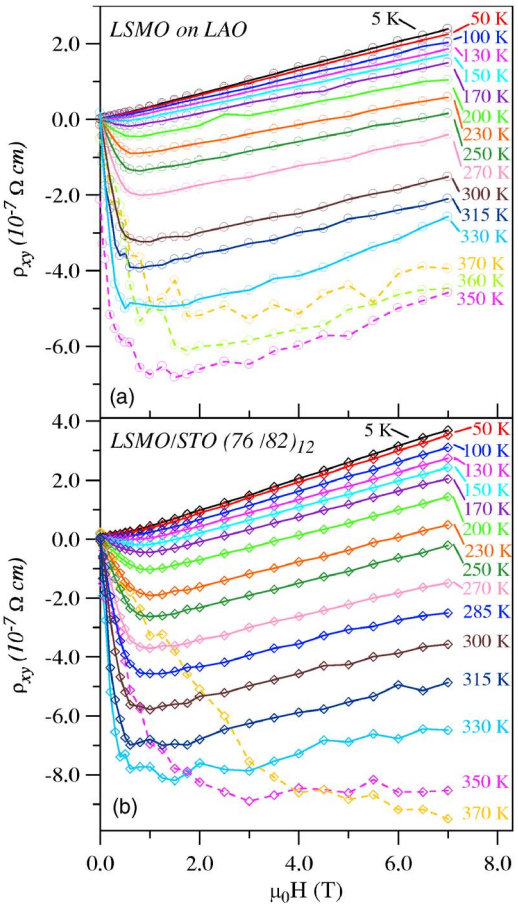

FIG. 9. (Color online) Transverse Hall resistivity ρ_{xy} vs applied field H for (a) the LSMO film deposited on LAO and (b) the $(76/82)_6$ superlattice at different temperatures.

can be expressed as $\rho_{xy}=R_oB+\mu_0R_sM$,[40] where R_o is the ordinary Hall coefficient, B is the magnetic induction, and R_s is the temperature-dependent anomalous Hall coefficient. We noted that $B=\mu_0[H+(1-N)M]$, where N is the demagnetization factor, and $N=1$ when the applied field is perpendicular to the film plane. From separate field-dependent magnetization measurements corrected for demagnetizing fields, the R_o and R_s for temperatures can be determined precisely as described previously.[39] The anomalous Hall effect (AHE) has been found to support the carrier-hopping mechanism and the scenario of the Berry-phase effects.[21] At this point, we further examine the Hall effect. Figure 10 shows the temperature dependence of effective carrier concentration N_{eff} extracted from the ordinary Hall coefficient R_o for LSMO/STO superlattices and the LSMO film deposited on LAO. As can be seen, when the temperature is increased from the low-temperature regime, most $N_{eff}(T)$ curves show a slight increase with temperature, going to a local maximum, and then showing a rapid drop at temperatures near T_C. This rapid decrease of N_{eff} corresponds to a cusplike behavior of $R_o(T)$ predicted by Majumdar *et al.*[41] due to $R_o=1/eN_{eff}$, which has also been observed on the $La_{0.67}Ca_{0.33}MnO_3$ and $Nd_{0.7}Sr_{0.3}MnO_3$ films.[38,39] It is noteworthy that in the low-temperature region the N_{eff} decreases for superlattice with thicker STO layers or thinner LSMO layers. The decrease of

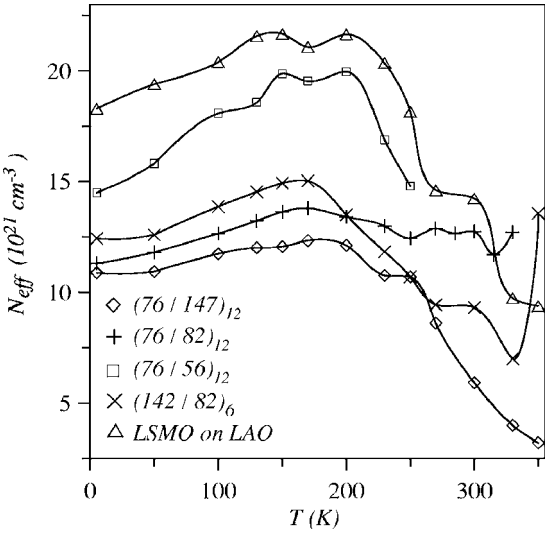

FIG. 10. Temperature dependence of effective carrier concentration N_{eff} extracted from the ordinary Hall coefficient R_o for LSMO/STO superlattices and the LSMO film deposited on LAO.

N_{eff} seems to be consistent with the increase in resistivity observed on the LSMO/STO superlattices with higher disorder. Moreover, the obtained values of N_{eff} at low temperatures for our LSMO/STO superlattices are close to those of $La_{1-x}Sr_xMnO_3$ crystals.[37] It may be worth pointing out, in passing, that in the high-temperature region the values of N_{eff} seem to show an unsystematic variation with the change of the layer thickness. This can be attributed to an additional contribution of the anomalous Hall effects, which is difficult to be separated accurately at temperatures near T_C.[42]

Figure 11 displays the typical scaling behavior of R_s versus zero-field ρ_{xx} curves for LSMO/STO superlattices and

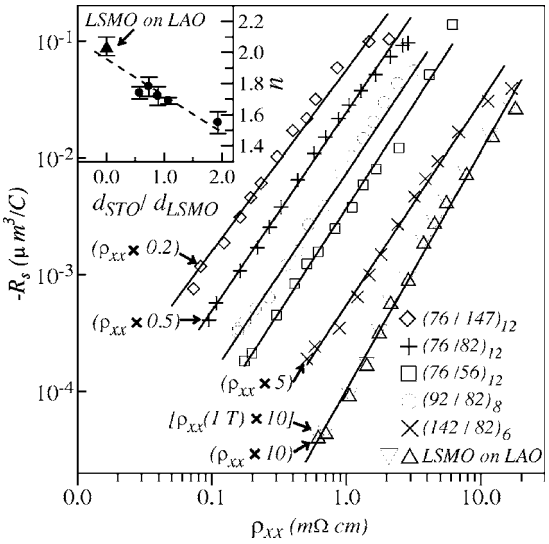

FIG. 11. Scaling behavior of R_s vs zero-field ρ_{xx} curves for LSMO/STO superlattices and the LSMO film deposited on LAO substrate. The solid lines express the scaling law $-R_s \propto (\rho_{xx})^n$. Some curves are horizontally shifted for clarity. The inset shows the obtained n values versus the d_{STO}/d_{LSMO} ratio and the dashed line is to serve as a visual guide.

the LSMO film deposited on an LAO substrate. It should be recalled here that in magnetic materials, there exists a correlation between R_s and ρ_{xx} expressed by $-R_s \propto (\rho_{xx})^n$. In classical theory, the exponent n is 1 for skew scattering and $n=2$ for side-jump processes.[43] Being different from those predicted with classical mechanisms, $n=1.2-2$ for the doped manganites has been observed experimentaly.[37,39] The inset of Fig. 11 shows the obtained n values versus the d_{STO}/d_{LSMO} ratio. As shown, n is in the range of 1.55–2.04 and generally decreases with a decrease of LSMO-layer thickness or an increase of spacer-layer thickness. We may note in passing that the scaling law remains the same even if we use the resistivity ρ_{xx} at an external field of 1 T as an example of the LSMO film, as shown in Fig. 11. Even though the qualitative variation in n for the LSMO/STO superlattices has been generally discussed previously,[21] it is still interesting to consider the origin of the variation in n among these superlattices in detail. Over the past few years, a considerable number of studies have been made on the AHE in multilayers or superlattices composed of conventional magnetic and nonmagnetic metals.[44–47] Many authors have shown scaling laws with the power $n>2$ and argued that the interface scattering plays an important role in the AHE. Furthermore a widely cited theoretical work on the AHE in multilayers or superlattices has been presented by Zhang,[48] which concentrates on the side jump as the main source for the AHE. Recently, another work by Gerber *et al.*[49] presented a different argument, which interpreted the AHE in terms of a modified skew scattering model. Even through there is no consensus on this subject for the magnetic-metal multilayers, in the superlattices composed of manganite we consider the side jump to be the main source for the AHE because their resistivities are usually much larger than those of magnetic metals.[38] Recalling the theory proposed by Zhang, we can see that the commonly used scaling law between R_s and ρ_{xx} for homogeneous magnetic materials is valid only under the local limit, that is, when the mean free path is much less than that of the layer thickness. He claimed that the scaling law is always invalid for the case of superlattices, since in such systems the mean free path is always larger than the layer thickness. Numerical analysis in his theory reveals that the exponent in the scaling law can be smaller than, greater than, or equal to 2, depending on the relative variations in the mean free path for the magnetic and the nonmagnetic layers. On the basis of Zhang's model, Canedy *et al.*[45] supposed that the interfaces would dominate the scattering and then the mean free path could scale as the layer thickness to explain the observed deviation from the conventional scaling law in their Co/Pt superlattices. Also, a larger exponent n for multilayers with higher interface roughness has been found by Korenivski *et al.*[44] For the LSMO/STO superlattices containing the conducting LSMO and insulating STO layers, however, the situation can be regarded as an inhomogeneous case because the electron sees an inhomogeneous scattering environment. By considering the interface scattering associated with the enhanced disorder in superlattices, it can be expected that the exponent n would deviate from 2. Our results seem to be similar in behavior to the situation for Co/Pt superlattices with the thickness of Co greater than that of Pt, corresponding to this case where mean free path in LSMO layers is much larger than that in STO layers, in which the exponent n deviating from 2 and becoming smaller was observed also.[45]

IV. SUMMARY

We have presented the crystalline structures, magnetisms, and magnetotransport properties of LSMO/STO superlattices and LSMO films. The LSMO films deposited on LAO and STO substrates reveal an out-of-plane tensile stress and an out-of-plane compressive stress, respectively. For LSMO/STO superlattices, we use direct observation of TEM images and provide evidence that the superlattices almost have the same in-plane stress while having a slight increase of out-of-plane strain in LSMO layers for superlattices with thicker STO layers. In the study of magnetic properties, the decreases both in Curie temperature and magnetization for superlattices with thicker STO or thinner LSMO layers have been observed, which can be attributed to the enhanced decoupling and magnetic disordering among the ferromagnetic LSMO layers. Furthermore, the longitudinal and transverse transport results provide insight into the effects of decoupling and magnetic disordering on the physical mechanism of the magnetotransport properties. We demonstrate that the temperature dependence of resistivity, the residual resistivity, the field dependence of MR, the Hund coupling, the effective carrier concentration, and the scaling behavior of anomalous Hall coefficient versus resistivity are dominated by the magnetic disorder associated with the magnon scattering in the LSMO/STO superlattices. We also note that both the single-layer LSMO films deposited on STO and LAO substrates have similar properties to their behavior regardless of their different strain types. Here, we do not intend to imply that the strain has no effect, but we can see that the strain effect has only a minor effect on the magnetotransport properties of the overall samples discussed here. Our results support the scenario that the interlayer decoupling increases the influence of disorder effects on the magnetism and the magnetotransport phenomenon in LSMO/STO superlattices.

ACKNOWLEDGMENT

The authors thank the National Science Council of the Republic of China for financial support under Grants No. NSC 94-2112-M-212-001, No. NSC 94-2623-7-212-003-AT, and No. NSC 95-2112-M-212-001-MY3.

[1] Yu Lu, X. W. Li, G. Q. Gong, Gang Xiao, A. Gupta, P. Lecoeur, J. Z. Sun, Y. Y. Wang, and V. P. Dravid, Phys. Rev. B **54**, R8357 (1996); J. S. Noh, T. K. Nath, C. B. Eom, J. Z. Sun, W. Tian, and X. Q. Pan, Appl. Phys. Lett. **79**, 233 (2001).
[2] Alvydas Lisauskas, S. I. Khartsev, and Alex Grishin, Appl. Phys. Lett. **77**, 756 (2000); Fan Yang, Laurence Méchin, Jean-Marc Routoure, Bruno Guillet, and Radoslav A. Chakalov, J. Appl. Phys. **99**, 024903 (2006).
[3] C. Zener, Phys. Rev. **82**, 403 (1951); P.-G. de Gennes, *ibid.* **118**, 141 (1960).
[4] M. B. Salamon and M. Jaime, Rev. Mod. Phys. **73**, 583 (2001).
[5] Y. M. Xiong, G. Y. Wang, X. G. Luo, C. H. Wang, X. H. Chen, X. Chen, and C. L. Chen, J. Appl. Phys. **97**, 083909 (2005).
[6] M. Ziese, H. C. Semmelhack, and K. H. Han, Phys. Rev. B **68**, 134444 (2003).
[7] M. Ziese, H. C. Semmelhack, K. H. Han, S. P. Sena, and H. J. Blythe, J. Appl. Phys. **91**, 9930 (2002).
[8] R. A. Rao, D. Lavric, T. K. Nath, C. B. Eom, L. Wu, and F. Tsui, Appl. Phys. Lett. **73**, 3294 (1998).
[9] Joseph Dvorak, Y. U. Idzerda, S. B. Ogale, Sanjay Shinde, Tao Wu, T. Venkatesan, R. Godfrey, and R. Ramesh, J. Appl. Phys. **97**, 10C102 (2005).
[10] Yafeng Lu, J. Klein, C. Höfener, B. Wiedenhorst, J. B. Philipp, F. Herbstritt, A. Marx, L. Alff, and R. Gross, Phys. Rev. B **62**, 15806 (2000).
[11] M. Izumi, Y. Ogimoto, Y. Okimoto, T. Manako, P. Ahmet, K. Nakajima, T. Chikyow, M. Kawasaki, and Y. Tokura, Phys. Rev. B **64**, 064429 (2001).
[12] I. Panagiotopoulos, C. Christides, M. Pissas, and D. Niarchos, Phys. Rev. B **60**, 485 (1999).
[13] L. M. Wang and Chih-Chian Guo, Appl. Phys. Lett. **87**, 172503 (2005).
[14] H. C. Yang, L. M. Wang, and H. E. Horng, Phys. Rev. B **59**, 8956 (1999).
[15] Michael C. Martin, G. Shirane, Y. Endoh, K. Hirota, Y. Moritomo, and Y. Tokura, Phys. Rev. B **53**, 14285 (1996).
[16] M. Sahana, T. Walter, K. Dörr, K.-H. Müller, D. Eckert, and K. Brand, J. Appl. Phys. **89**, 6834 (2001).
[17] O. I. Lebedev, J. Verbeeck, G. Van Tendeloo, C. Dubourdieu, M. Rosina, and P. Chaudouët, J. Appl. Phys. **94**, 7646 (2003).
[18] H.-U. Habermeier, Physica B **321**, 9 (2002).
[19] S. Jacob, T. Roch, F. S. Razavi, G. M. Gross, and H.-U. Habermeier, J. Appl. Phys. **91**, 2232 (2002).
[20] M. Bibes, Ll. Balcells, S. Valencia, J. Fontcuberta, M. Wojcik, E. Jedryka, and S. Nadolski, Phys. Rev. Lett. **87**, 067210 (2001).
[21] L. M. Wang, Phys. Rev. Lett. **96**, 077203 (2006).
[22] M. Sirena, N. Haberkorn, M. Granada, L. B. Steren, and J. Guimpel, J. Appl. Phys. **93**, 7244 (2003).
[23] Prahallad Padhan and R. C. Budhani, Phys. Rev. B **71**, 144415 (2005).
[24] N. Akiba, F. Matsukura, A. Shen, Y. Ohno, H. Ohno, A. Oiwa, S. Katsumoto, and Y. Iye, Appl. Phys. Lett. **73**, 2122 (1998); D. Chiba, N. Akiba, F. Matsukura, Y. Ohno, and H. Ohno, *ibid.* **77**, 1873 (2000).
[25] A. Urushibara, Y. Moritomo, T. Arima, A. Asamitsu, G. Kido, and Y. Tokura, Phys. Rev. B **51**, 14103 (1995).
[26] M. Jaime, P. Lin, M. B. Salamon, and P. D. Han, Phys. Rev. B **58**, R5901 (1998).
[27] Guo-meng Zhao, V. Smolyaninova, W. Prellier, and H. Keller, Phys. Rev. Lett. **84**, 6086 (2000).
[28] L. M. Wang, H. C. Yang, and H. E. Horng, Phys. Rev. B **64**, 224423 (2001).
[29] G. J. Snyder, Ron Hiskes, Steve DiCarolis, M. R. Beasley, and T. H. Geballe, Phys. Rev. B **53**, 14434 (1996).
[30] T. Akimoto, Y. Moritomo, A. Nakamura, and N. Furukawa, Phys. Rev. Lett. **85**, 3914 (2000).
[31] X. J. Chen, H.-U. Habermeier, C. L. Zhang, H. Zhang, and C. C. Almasan, Phys. Rev. B **67**, 134405 (2003).
[32] Yu. A. Boĭkov, T. Claeson, and V. A. Danilov, Phys. Solid State **47**, 2281 (2005).
[33] S. Mercone, C. A. Perroni, V. Cataudella, C. Adamo, M. Angeloni, C. Aruta, G. De Filippis, F. Miletto, A. Oropallo, P. Perna, Y. Petrov, U. S. di Uccio, and L. Maritato, Phys. Rev. B **71**, 064415 (2005).
[34] L. M. Wang, H. E. Horng, and H. C. Yang, Phys. Rev. B **70**, 014433 (2004).
[35] R. Mathieu, P. Svedlindh, R. A. Chakalov, and Z. G. Ivanov, Phys. Rev. B **62**, 3333 (2000).
[36] N. Furukawa, J. Phys. Soc. Jpn. **63**, 3214 (1994).
[37] A. Asamitsu and Y. Tokura, Phys. Rev. B **58**, 47 (1998).
[38] G. Jakob, F. Martin, W. Westerburg, and H. Adrian, Phys. Rev. B **57**, 10252 (1998).
[39] H. C. Yang, L. M. Wang, and H. E. Horng, Phys. Rev. B **64**, 174415 (2001).
[40] C. M. Hurd, *The Hall Effect in Metals and Alloys* (Plenum, New York, 1972).
[41] Pinaki Majumdar, Steven H. Simon, and Anirvan M. Sengupta, Phys. Rev. B **59**, 4746 (1999).
[42] P. Matl, N. P. Ong, Y. F. Yan, Y. Q. Li, D. Studebaker, T. Baum, and G. Doubinina, Phys. Rev. B **57**, 10248 (1998).
[43] L. Berger and G. Bergmann, in *The Hall Effect and Its Applications*, edited by C. L. Chien and C. R. Westgate (Plenum, New York, 1980), p. 55.
[44] V. Korenivski, K. V. Rao, J. Colino, and Ivan K. Schuller, Phys. Rev. B **53**, R11938 (1996).
[45] C. L. Canedy, X. W. Li, and Gang Xiao, Phys. Rev. B **62**, 508 (2000).
[46] P. Khatua, A. K. Majumdar, A. F. Hebard, and D. Temple, Phys. Rev. B **68**, 144405 (2003).
[47] P. Khatua, A. K. Majumdar, D. Temple, and C. Pace, Phys. Rev. B **73**, 094421 (2006).
[48] Shufeng Zhang, Phys. Rev. B **51**, 3632 (1995).
[49] A. Gerber, A. Milner, A. Finkler, M. Karpovski, L. Goldsmith, J. Tuaillon-Combes, O. Boisron, P. Mélinon, and A. Perez, Phys. Rev. B **69**, 224403 (2004).